Progress In Electromagnetics Research C, Vol. 83, 97–111, 2018

Reconstruction of 3D Anisotropic Objects by VIE and Model-Based Inversion Methods

Lin E. Sun[1, *] and Mei Song Tong[2]

Abstract—A model-based inversion algorithm combined with the curl-conforming volume integral equation method is presented for the reconstruction of 3D anisotropic objects. The forward algorithm utilizes the curl-conforming volume integral equation method. The inversion algorithm is based on the Gauss-Newton method. The approach is applied to the reconstruction of the permittivities of 3D anisotropic objects. Moreover, sensitivity analysis of the data from different polarizations of transmitters and receivers to the anisotropic properties is performed. Numerical examples show the effectiveness of the inversion algorithm and demonstrate the sensitivities of data from different transmitter and receiver pairs to the anisotropy.

1. INTRODUCTION

Inverse scattering methods have been used in the reconstruction of objects in various areas such as subsurface sensing, biomedical imaging and nondestructive evaluation for decades. The scatter properties such as conductivity, permittivity and permeability, and location and shape are reconstructed from the scattered electromagnetic fields. There are mainly two categories of inversion methods. One is the pixel-based method. In this method, the inverted parameters are the material properties, such as the permittivity and conductivity in each pixel. It is very suitable for objects with highly inhomogeneous media [1–3, 5]. The other category of method is model-based method. In this method, the inversion domain is divided into regions. The shapes of different regions are described using geometrical parameters. The inverted parameters are the shapes of regions and the material properties for each region. Compared to the pixel-based method, model-based method is often more efficient since the number of inverted parameters is highly reduced, and the *a priori* information is used [6, 8, 9].

Analysis of scattering from anisotropic materials has been of great interest due to its wide application in subsurface sensing, metamaterials, etc. Among various numerical methods, a curl-conforming volume integral equation (VIE) method has been proposed to model the scattering from anisotropic objects [10]. Although much work has been done on the inversion of anisotropic objects using tri-axial transmitters and receivers in the subsurface sensing area [6, 7], inversion of anisotropic objects in free space is still limited. In the literature work for the reconstruction of 3D dielectric objects in free space, most of the previous work handles the isotropic objects only.

In this paper, we propose a combined method of VIE and model-based inversion method to solve the reconstruction of 3D anisotropic objects. The forward method employs the curl-conforming VIE method for anisotropic objects proposed in [10]. The inversion method is based on the multiplicatively regularized Gauss-Newton Method [4]. It is well known that the inverse scattering problem is nonlinear and ill-posed. Hence, to solve the inverse scattering problem for the anisotropic objects, it is essential to perform the sensitivity analysis for the measurements. Finally, in the numerical results part, we

Received 10 January 2018, Accepted 22 March 2018, Scheduled 11 April 2018

* Corresponding author: Lin E. Sun (lsun@ysu.edu).

[1] Department of Electrical and Computer Engineering, Youngstown State University, Youngstown, OH 44512, USA. [2] Department of Electronic Science and Technology, Tongji University, Shanghai, China.

demonstrate the sensitivity analysis of different measurements to the anisotropic permittivities. We also show the reconstruction results of anisotropic permittivities. It is proved that the proposed forward and inversion methods are capable and efficient for the reconstruction of 3D anisotropic objects.

2. FORWARD SCATTERING PROBLEM

Consider a 3D inhomogeneous and anisotropic object in free space with relative permittivity $\overline{\boldsymbol{\epsilon}}_r(\mathbf{r})$ and relative permeability $\overline{\boldsymbol{\mu}}_r(\mathbf{r})$. The object is illuminated by either a plane wave or a field excited by a dipole source indicated as T in Fig. 1. The receivers denoted as R are located in a plane. For each incident field, the total field $\mathbf{E}(\mathbf{r})$ is solved from the following volume integral equation [10]

$$\begin{aligned}\mathbf{E}(\mathbf{r}) \;=\; & \mathbf{E}^{inc}(\mathbf{r}) + k_0^2 \int_{V^+} \overline{\mathbf{G}}(\mathbf{r},\mathbf{r}') \cdot \left[\overline{\boldsymbol{\epsilon}}_r(\mathbf{r}') - \overline{\mathbf{I}}\right] \cdot \mathbf{E}(\mathbf{r}') d\mathbf{r}' \\ & -\nabla \times \int_{V^+} g(\mathbf{r},\mathbf{r}') \left[\overline{\boldsymbol{\mu}}_r^{-1}(\mathbf{r}') - \overline{\mathbf{I}}\right] \cdot \nabla' \times \mathbf{E}(\mathbf{r}') d\mathbf{r}' \end{aligned} \tag{1}$$

Here, V^+ represents the volume that is slightly larger than the volume of the object V. $\overline{\mathbf{G}}(\mathbf{r},\mathbf{r}')$ is the dyadic Green's function for the unbounded and homogeneous medium. It satisfies the following equation

$$\nabla \times \nabla \times \overline{\mathbf{G}}(\mathbf{r},\mathbf{r}') - k_0^2 \overline{\mathbf{G}}(\mathbf{r},\mathbf{r}') = \overline{\mathbf{I}} \delta(\mathbf{r}-\mathbf{r}') \tag{2}$$

and given by

$$\overline{\mathbf{G}}(\mathbf{r},\mathbf{r}') = \left(\overline{\mathbf{I}} + \frac{\nabla\nabla}{k_0^2}\right) g(\mathbf{r},\mathbf{r}') \tag{3}$$

where $g(\mathbf{r},\mathbf{r}')$ is the scalar Green's function, and k_0 is the wave number in free space.

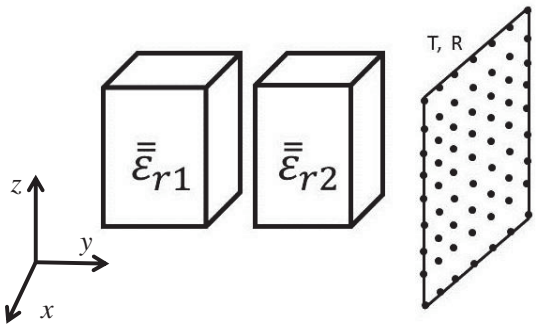

Figure 1. Configuration of the inverse problem and measurement setup.

To solve the volume integral equation in Eq. (1) by method of moments, we need to convert it into a set of linear algebraic equations. First, we discretize the volume of the object into a sum of tetrahedrons, and each tetrahedron is specified by 4 nodes and 6 edges. Next, we use the first-order edge basis defined on each edge of the tetrahedrons to discretize the unknown fields [11]. Hence, the electric field $\mathbf{E}(\mathbf{r})$ can be expanded into discretized forms as

$$\mathbf{E}(\mathbf{r}) = \sum_{i=1}^{N_e} I_i \mathbf{N}_i(\mathbf{r}), \quad \mathbf{r} \in V \tag{4}$$

Inserting (4) into (1), we have the discretized form of Equation (1)

$$\begin{aligned} -\mathbf{E}^{inc}(\mathbf{r}) \;=\; & -\sum_{i=1}^{N_e} I_i \mathbf{N}_i(\mathbf{r}) + k_0^2 \sum_{i=1}^{N_e} I_i \int_{V^+} \overline{\mathbf{G}}(\mathbf{r},\mathbf{r}') \cdot \left[\overline{\boldsymbol{\epsilon}}_r(\mathbf{r}') - \overline{\mathbf{I}}\right] \cdot \mathbf{N}_i(\mathbf{r}') d\mathbf{r}' \\ & -\sum_{i=1}^{N_e} I_i \nabla \times \int_{V^+} g(\mathbf{r},\mathbf{r}') \left[\overline{\boldsymbol{\mu}}_r(\mathbf{r}') - \overline{\mathbf{I}}\right] \cdot \nabla' \times \mathbf{N}_i(\mathbf{r}') d\mathbf{r}' \end{aligned} \tag{5}$$

Using the Galerkin's method and testing Eq. (5) using edge bases, we can convert the discretized volume integral equation to a linear matrix equation

$$\left[\mathbf{e}^{inc}\right] = \left[\overline{\mathbf{Z}}\right] \cdot [\mathbf{I}] \tag{6}$$

where the matrix element is given by

$$\left(\overline{\mathbf{Z}}\right)_{ji} = \left(\overline{\mathbf{Z}}\right)^{i}_{ii} + \left(\overline{\mathbf{Z}}^{\epsilon}\right)_{ji} + \left(\overline{\mathbf{Z}}^{\mu}\right)_{ji} \tag{7}$$

$$\left(\overline{\mathbf{Z}}^{i}\right)_{ii} = -\left\langle \mathbf{N}_j(\mathbf{r}), \mathbf{N}_i(\mathbf{r})\right\rangle \tag{8}$$

$$\left(\overline{\mathbf{Z}}^{\epsilon}\right)_{ji} = k_0^2 \left\langle \mathbf{N}_j(\mathbf{r}), \overline{\mathbf{G}}(\mathbf{r},\mathbf{r}') \cdot \left[\overline{\boldsymbol{\epsilon}}_r(\mathbf{r}') - \overline{\mathbf{I}}\right], \mathbf{N}_i(\mathbf{r}')\right\rangle \tag{9}$$

$$\left(\overline{\mathbf{Z}}^{\mu}\right)_{ji} = -\left\langle \mathbf{N}_j(\mathbf{r}), \nabla \times g(\mathbf{r},\mathbf{r}') \left[\overline{\boldsymbol{\mu}}_r^{-1}(\mathbf{r}') - \overline{\mathbf{I}}\right], \nabla \times \mathbf{N}_i(\mathbf{r}')\right\rangle \tag{10}$$

By solving matrix Equation (6) using the iterative method GMRES, the total electric field in the whole solution domain can be obtained.

The scattered electric field measured at R in Fig. 1 is given by

$$\begin{aligned}\mathbf{E}^{sca}(\mathbf{r}_j) = {} & k_0^2 \int_{V^+} \overline{\mathbf{G}}(\mathbf{r}_j,\mathbf{r}') \cdot \left[\overline{\boldsymbol{\epsilon}}_r(\mathbf{r}') - \overline{\mathbf{I}}\right] \cdot \mathbf{E}(\mathbf{r}') d\mathbf{r}' \\ & - \int_{V^+} \overline{\mathbf{G}}(\mathbf{r}_j,\mathbf{r}') \cdot \nabla' \times \left[\overline{\boldsymbol{\mu}}_r^{-1}(\mathbf{r}') - \overline{\mathbf{I}}\right] \cdot \nabla' \times \mathbf{E}(\mathbf{r}') d\mathbf{r}'\end{aligned} \tag{11}$$

and the total electric field in this equation is solved using MOM method introduced above. Here $\mathbf{r}_j$ represents the position of the j-th receiver, $j = 1, 2, \ldots, M'$, and M' is the number of receivers.

3. INVERSION ALGORITHM

The inverse problem is governed by Eqs. (1) and (11). In order to solve for $(\overline{\boldsymbol{\epsilon}}_r(\mathbf{r}') - \overline{\mathbf{I}})$ in Eq. (11), we consider the inverse scattering problem as an optimization problem, where it can be solved by minimizing the following cost function

$$C(\mathbf{x}) = \frac{1}{2}\left\{\overline{\mathbf{W}}_d \cdot \left\|\mathbf{E}^{sca}(\mathbf{x}) - \mathbf{E}^{d}\right\|^2 + \lambda \overline{\mathbf{W}}_m \cdot \|(\mathbf{x} - \mathbf{x}_p)\|^2\right\} \tag{12}$$

Here, the first term is the difference of the simulated scattered fields and the measured data, which represents the data misfit. In the above, $\mathbf{E}^{sca}(\mathbf{x})$ denotes the vector of simulated scattered field, and $\mathbf{E}^{d}$ denotes the vector of measured data. The second term is the difference of the model parameters and their prescribed values. Here, $\mathbf{x}$ denotes the vector of model parameters $(\overline{\boldsymbol{\epsilon}}_r(\mathbf{r}') - \overline{\mathbf{I}})$. $\mathbf{x}_p$ denotes the prescribed model parameters. Since the a prior information about the model parameters is assumed unknown in this work, $\mathbf{x}_p$ is chosen as the model parameters in the previous step. $\overline{\mathbf{W}}_d$ is the data weighting matrix, which is chosen as the identity in this work. Note that when the noises for different measurements are different from each other, the diagonal terms of $\overline{\mathbf{W}}_d$ may need to take different values based on the noises. $\overline{\mathbf{W}}_m$ is the model weighting matrix, which is chosen as the identity as well in this work. In both terms of the cost function, L_2 norm is assumed. In the second term, λ is the regularization factor defined as a function that is proportional to the data mismatch

$$\lambda = \frac{1}{2}\alpha \left\|\mathbf{E}^{sca}(\mathbf{x}) - \mathbf{E}^{d}\right\|^2 \tag{13}$$

Here α is a constant mainly determined from test. In this work, it is chosen as 0.01. It is also noted that when there is noise in the data, the data mismatch term in the cost function will converge to a certain value depending on the noise level. Hence, larger values for α will be needed.

Upon minimizing the above cost function, we use the multiplicatively regularized Gauss-Newton method and obtain the linear equation as below [4]

$$\overline{\mathbf{H}}_k \cdot \delta\mathbf{x}_k = -\mathbf{g}_k \tag{14}$$

Here, $\overline{\mathbf{H}}_k$ denotes the Hessian matrix given by

$$\overline{\mathbf{H}}_k = \overline{\mathbf{J}}_k^T \cdot \overline{\mathbf{W}}_d^T \cdot \overline{\mathbf{W}}_d \cdot \overline{\mathbf{J}}_k + \lambda \overline{\mathbf{W}}_m^T \cdot \overline{\mathbf{W}}_m \tag{15}$$

and $\mathbf{g}_k$ denotes the gradient vector given by

$$\mathbf{g}_k = \overline{\mathbf{J}}_k^T \cdot \overline{\mathbf{W}}_d^T \cdot \overline{\mathbf{W}}_d \cdot \left(\mathbf{E}^{sca}(\mathbf{x}_k) - \mathbf{E}^d \right) + \lambda \overline{\mathbf{W}}_m^T \cdot \overline{\mathbf{W}}_m \left(\mathbf{x}_k - \mathbf{x}_p \right) \tag{16}$$

In the above, $\overline{\mathbf{J}}_k$ is the Jacobian matrix at the k-th iteration. The mn-th element in the Jacobian is computed using the derivative of the simulated data $\mathbf{E}_m^{sca}$ with respect to the model parameters x_n

$$J_{mn} = \frac{\partial \mathbf{E}_m^{sca}}{\partial x_n} = \frac{\mathbf{E}_m^{sca}((1+\delta)x_n) - \mathbf{E}_m^{sca}(x_n)}{\delta x_n} \tag{17}$$

Here, x_n is the n-th component of the model parameter vector $\mathbf{x}$. $\mathbf{E}_m^{sca}$ is the m-th component of the simulated data vector $\mathbf{s}$. δ is a small value chosen as 0.01.

In Equation (14), $\delta \mathbf{x}_k$ denotes the step vector at the k-th step. From the solution for $\delta \mathbf{x}_k$, we can solve the model parameter $\mathbf{x}_{k+1}$. This process continues until the solution converges. The iteration process will be terminated as one of the three conditions occurs first: i) The number of iterations exceeds a prescribed maximum; ii) The difference between the cost function at two successive iterates is within the tolerance 10^{-4}; iii) The difference between the model parameters at two successive iterates is within the tolerance 10^{-4}.

4. NUMERICAL RESULTS

Two anisotropic cubes as shown in Fig. 1 are excited by an electric diploe. The centers of the two cubes are located at $(0.5, 0.25, 0.5)$ m and $(0.5, 0.95, 0.5)$ m. The side length of each cube is $(1.0, 0.5, 1.0)$ m. Each cube is discretized into 852 tetrahedrons and 1,315 edge bases. The dipole is located at $(0.5, 1.5, 0.5)$ m. The receivers are also electric dipoles, and they are in the x-z plane at $y = 3.0$ m, along the x and z axes from -3.0 m to 3.0 m at every 0.3 m. The total number of receivers is 441. The frequency is 0.1 GHz. The relative permittivities are uniaxial tensors with $\overline{\boldsymbol{\epsilon}}_r = \begin{pmatrix} \epsilon_r & 0 & 0 \\ 0 & \epsilon_r & 0 \\ 0 & 0 & \epsilon_{rz} \end{pmatrix}$.

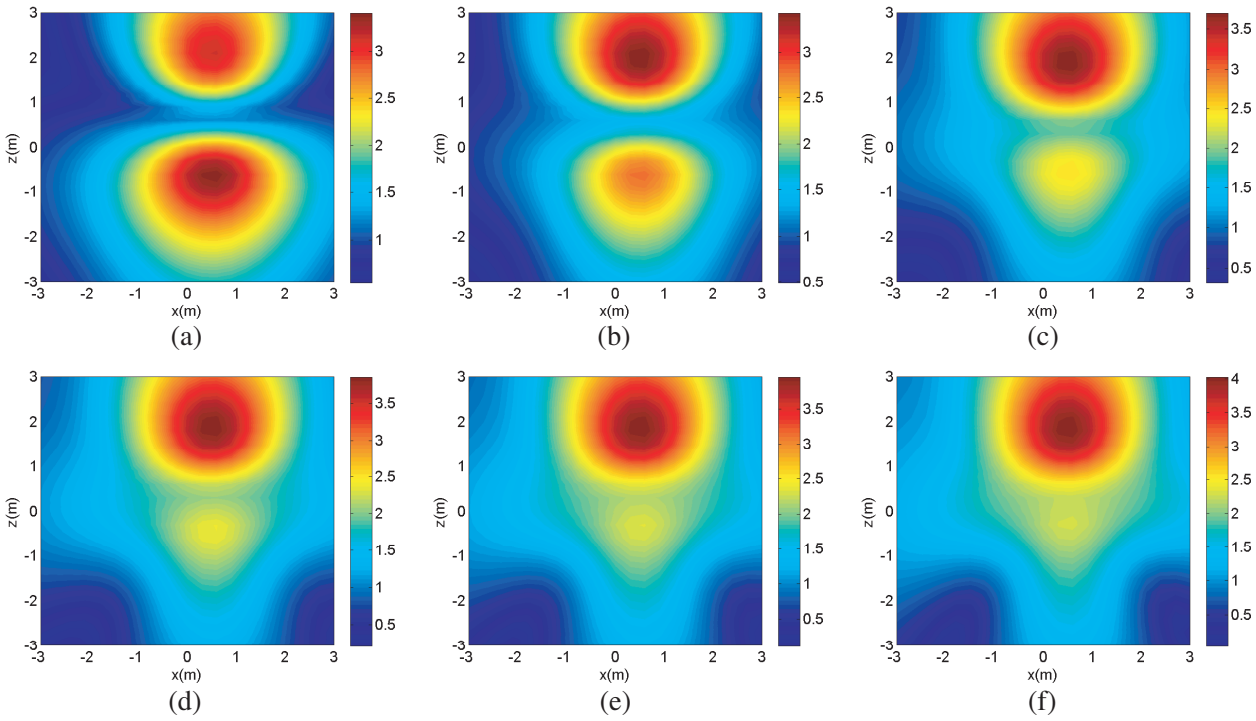

Figure 2. Scattered electric field of y-x polarization for different anisotropy ratios. (a) $\epsilon_{r1z} = 2$, (b) $\epsilon_{r1z} = 4$, (c) $\epsilon_{r1z} = 8$, (d) $\epsilon_{r1z} = 12$, (e) $\epsilon_{r1z} = 16$, (f) $\epsilon_{r1z} = 20$.

4.1. Example 1: Sensitivity Analysis

For cube 2, $\epsilon_{r2} = 4.0$, $\epsilon_{r2z} = 2.0$. For cube 1, $\epsilon_{r1} = 2.0$. For the examination of the sensitivity of measurements to the anisotropy, ϵ_{r1z} are chosen as 2, 4, 8, 12, 16, 20, respectively. Then the scattered fields in the receiver plane are plotted for each case. Fig. 2 shows that the scattered fields for the transmitter are y-polarized, and receivers are x-polarized. Fig. 3 shows that the scattered fields for the transmitter are z-polarized, and receivers are still x-polarized. We can see that the z-x polarized measurements are more sensitive to the change of the ratio $\epsilon_{r1z}/\epsilon_{r1}$.

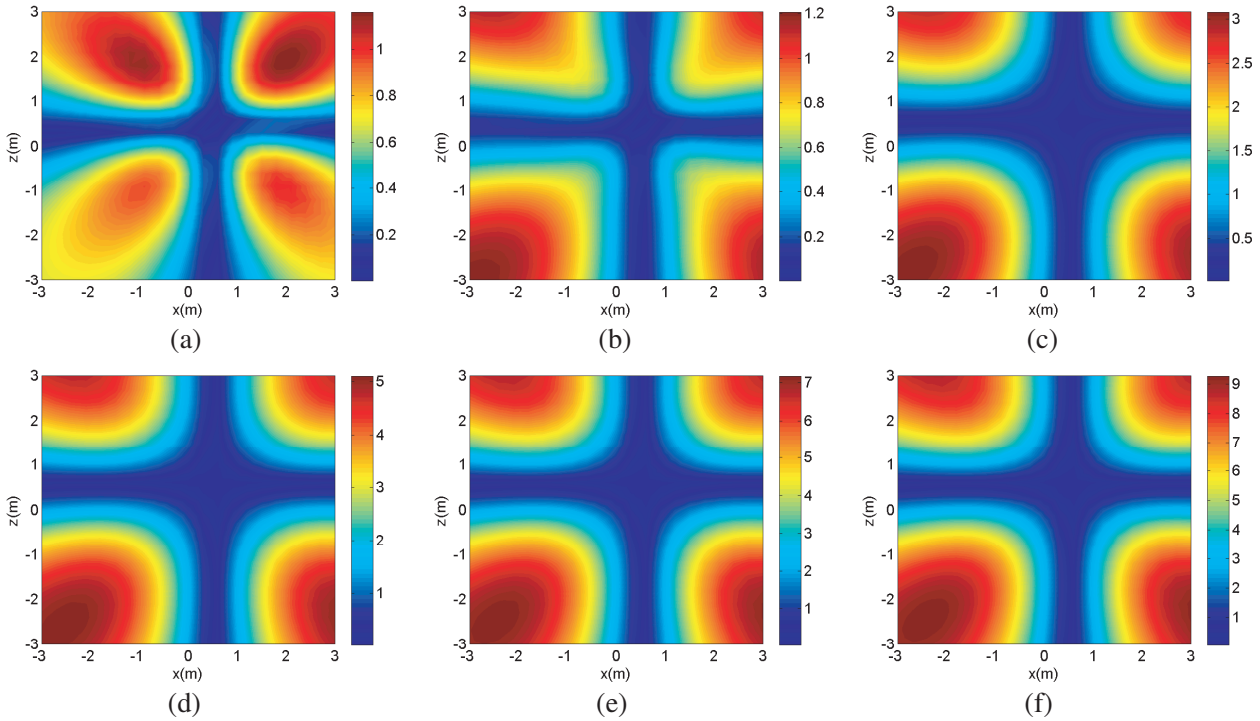

Figure 3. Scattered electric field of z-x polarization for different anisotropy ratios. (a) $\epsilon_{r1z} = 2$, (b) $\epsilon_{r1z} = 4$, (c) $\epsilon_{r1z} = 8$, (d) $\epsilon_{r1z} = 12$, (e) $\epsilon_{r1z} = 16$, (f) $\epsilon_{r1z} = 20$.

4.2. Example 2: Reconstruction of Isotropic Permittivities

In this example, we consider that both cubes are isotropic dielectrics. The relative permittivity of the left cube is $\epsilon_{r1} = 2$, and the relative permittivity of right cube is $\epsilon_{r2} = 4$. First, the receivers are placed on the same side of the transmitter at $y = 3.0$ m. The transmitter is polarized in $-y$ and z directions, and the receivers are polarized in x, y and z directions, respectively. Next, we will show the numerical results for both the noiseless and noisy data. For the noisy data, 25 dB (5.6 percents) signal-to-noise ratio (SNR) is applied to the data. The initial guess for the contrast of the relative permittivity is 1.0.

Figure 4 shows the reconstructed permittivities of the two cubes using the magnitude of the scattered electric field for different transmitter-receiver polarizations for both the noiseless and noisy cases. Next, we place the receivers at $y = -3.0$ m, on the different side of the transmitter. Fig. 5 shows the inverted results. From Figs. 4 and 5, we can see that all the results converge to actual values within 5 steps for the isotropic permittivities for both the noiseless and noisy data.

Next, we plot the cost function (CF) and data mismatch (DM) for different cases. Here the data mismatch (DM) is defined as the ratio of the norm of the difference of reconstructed data and measurements with the norm of the measurements.

$$DM = \frac{\left\|\mathbf{E}^{sca}(\mathbf{x}) - \mathbf{E}^{d}\right\|}{\left\|\mathbf{E}^{d}\right\|} \tag{18}$$

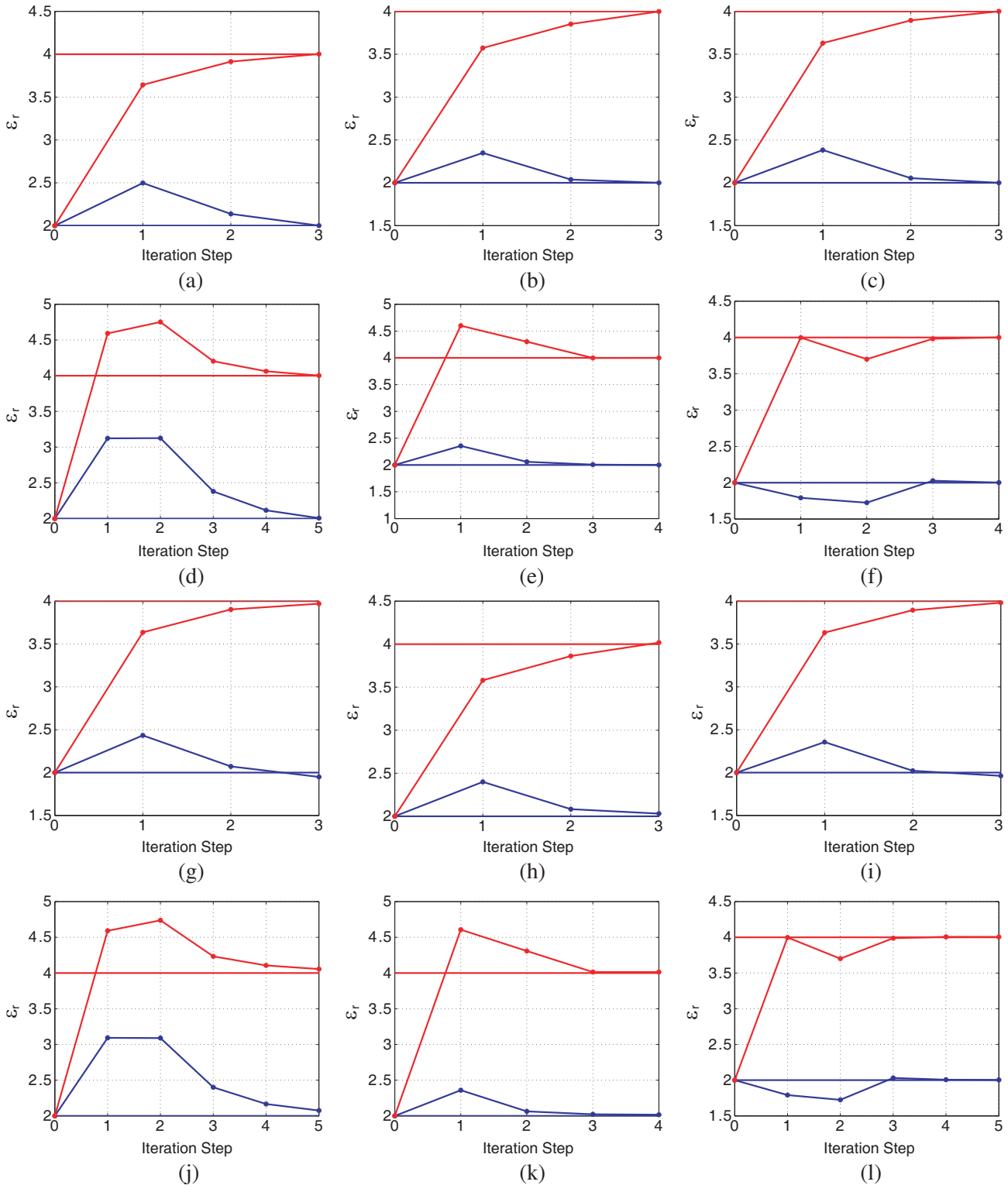

Figure 4. Inverted relative permittivities for isotropic cubes from different transmitter-receiver polarizations when the receivers are at $y = 3.0\,\mathrm{m}$ and the transmitter is at $(0.5, 1.5, 0.5)\,\mathrm{m}$: solid line actual values, dotted line inverted values, blue line ϵ_{r1}, red line ϵ_{r2}. The first two rows: noiseless data; the last two rows: noisy data. (a) y-x, (b) y-y, (c) y-z, (d) z-x, (e) z-y, (f) z-z, (g) y-x, (h) y-y, (i) y-z, (j) z-x, (k) z-y, (l) z-z.

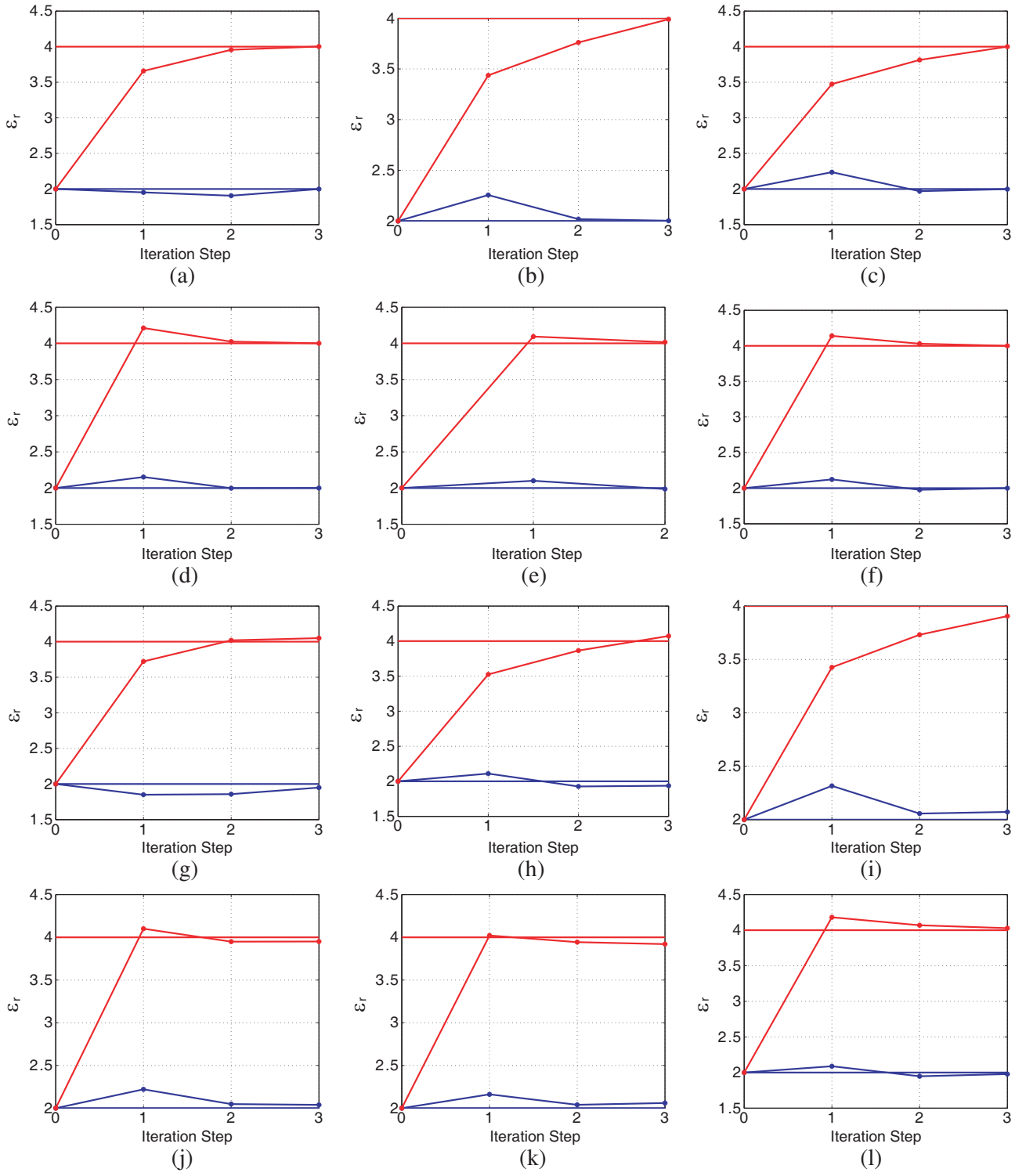

Figure 5. Inverted relative permittivities for isotropic cubes from different transmitter-receiver polarizations when the receivers are at $y = -3.0\,\mathrm{m}$ and the transmitter is at $(0.5, 1.5, 0.5)\,\mathrm{m}$: solid line actual values, dotted line inverted values, blue line ϵ_{r1}, red line ϵ_{r2}. The first two rows: noiseless data; the last two rows: noisy data. (a) y-x, (b) y-y, (c) y-z, (d) z-x, (e) z-y, (f) z-z, (g) y-x, (h) y-y, (i) y-z, (j) z-x, (k) z-y, (l) z-z.

Figure 6 shows the CF and DM as the function of iteration step when the transmitter and receivers are on the same side. Fig. 7 shows the CF and DM as the function of iteration step when the transmitter and receivers are on the opposite sides. For both cases, the cost functions converge to very small values. As for the DM, it is shown that the DM value can converge to very small values for the noiseless

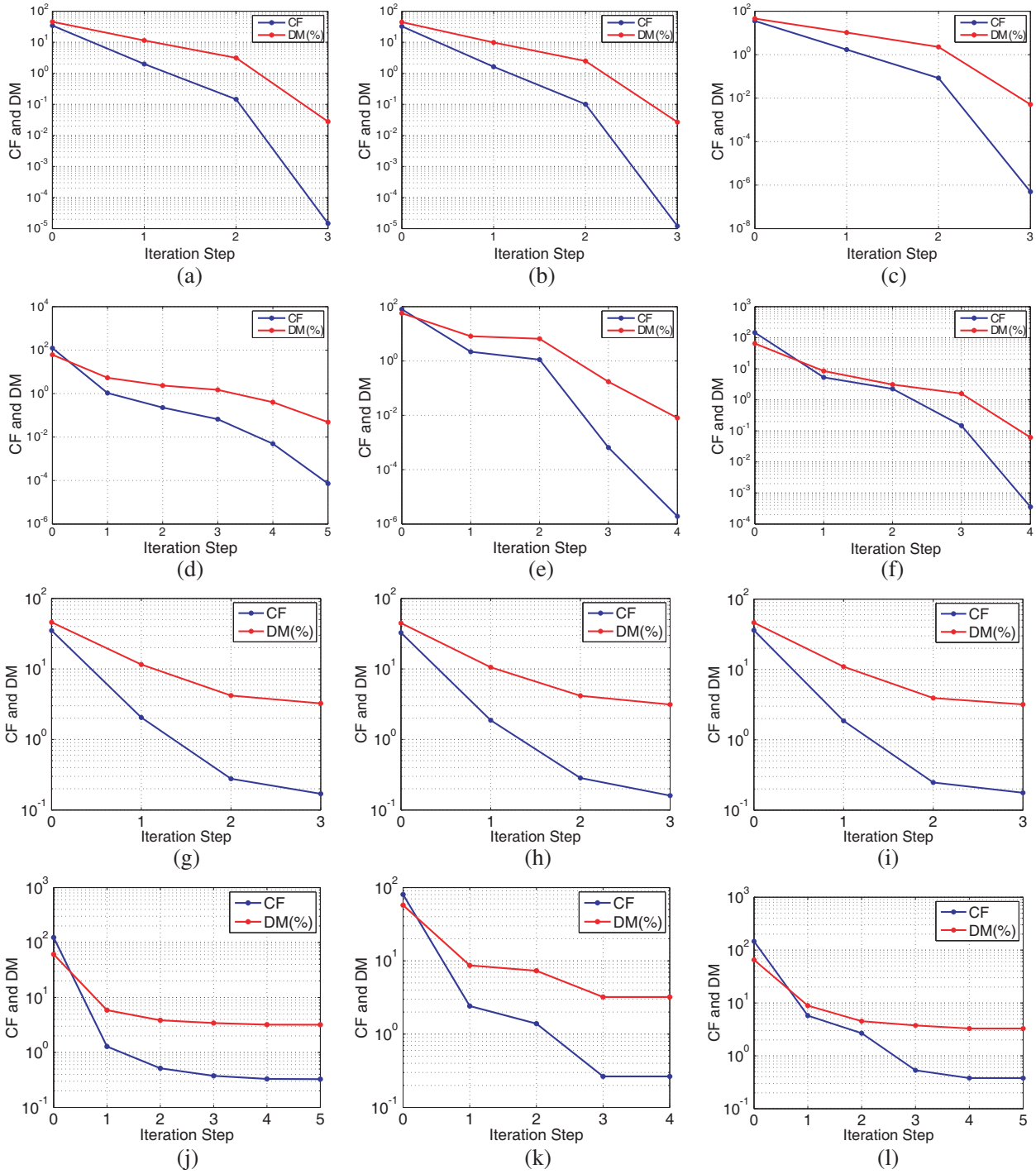

Figure 6. Cost function and data mismatch using data from different transmitter-receiver polarizations when the receivers are at $y = 3.0\,\mathrm{m}$ and the transmitter is at $(0.5, 1.5, 0.5)\,\mathrm{m}$ for isotropic cubes: blue line CF, red line DM (%). First two rows: noiseless data; last two rows: noisy data. (a) y-x, (b) y-y, (c) y-z, (d) z-x, (e) z-y, (f) z-z, (g) y-x, (h) y-y, (i) y-z, (j) z-x, (k) z-y, (l) z-z.

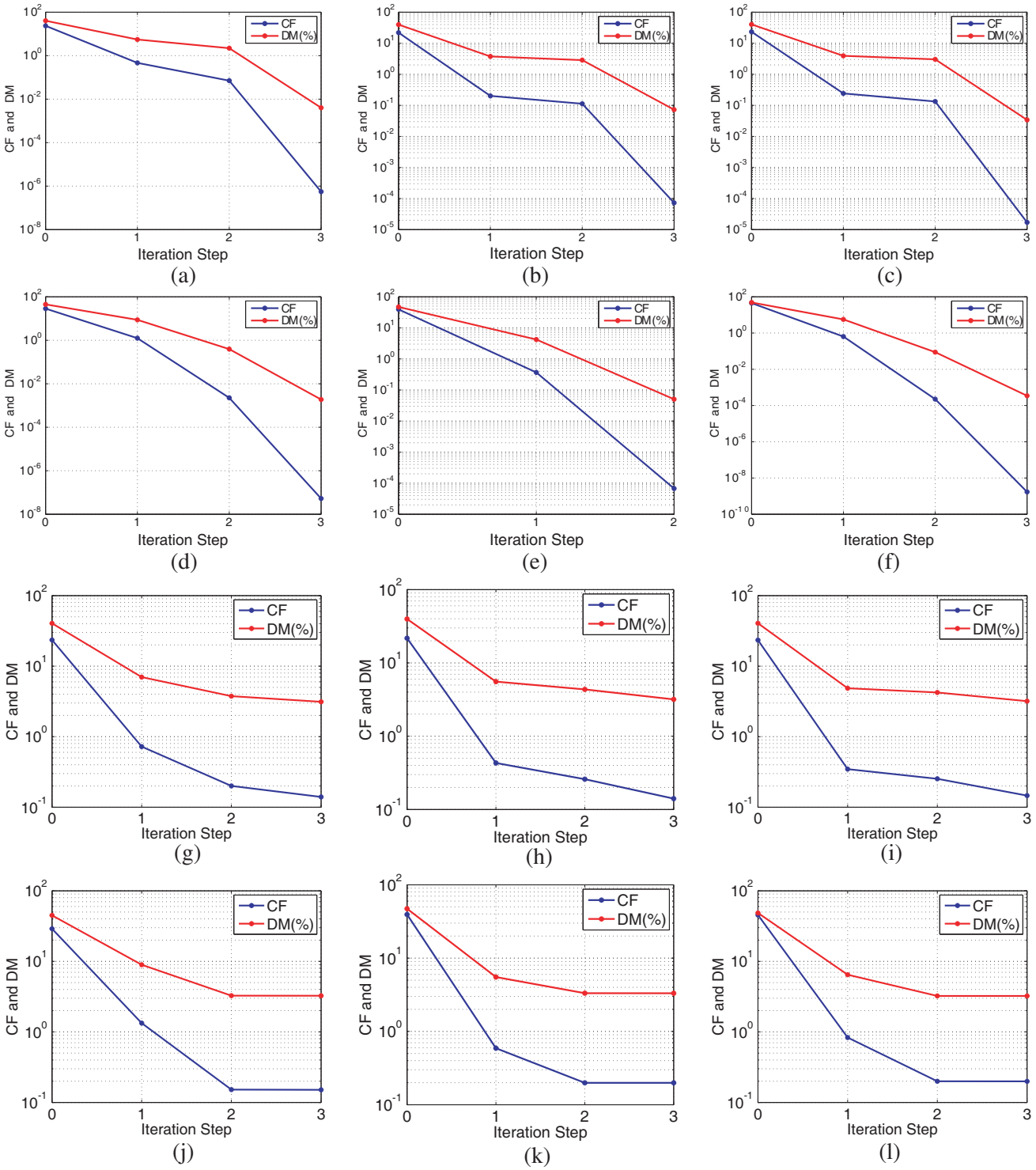

Figure 7. Cost function and data mismatch using data from different transmitter-receiver polarizations when the receivers are at $y = -3.0\,\mathrm{m}$ and the transmitter is at $(0.5, 1.5, 0.5)\,\mathrm{m}$ for isotropic cubes: blue line CF, red line DM (%). First two rows: noiseless data; last two rows: noisy data. (a) y-x, (b) y-y, (c) y-z, (d) z-x, (e) z-y, (f) z-z, (g) y-x, (h) y-y, (i) y-z, (j) z-x, (k) z-y, (l) z-z.

case. While for the noisy data, due to the noise added in the measurement data, the DM value cannot converge to very small values. For most of the cases, it converges to about 5%, which is the percent of noise added to the data.

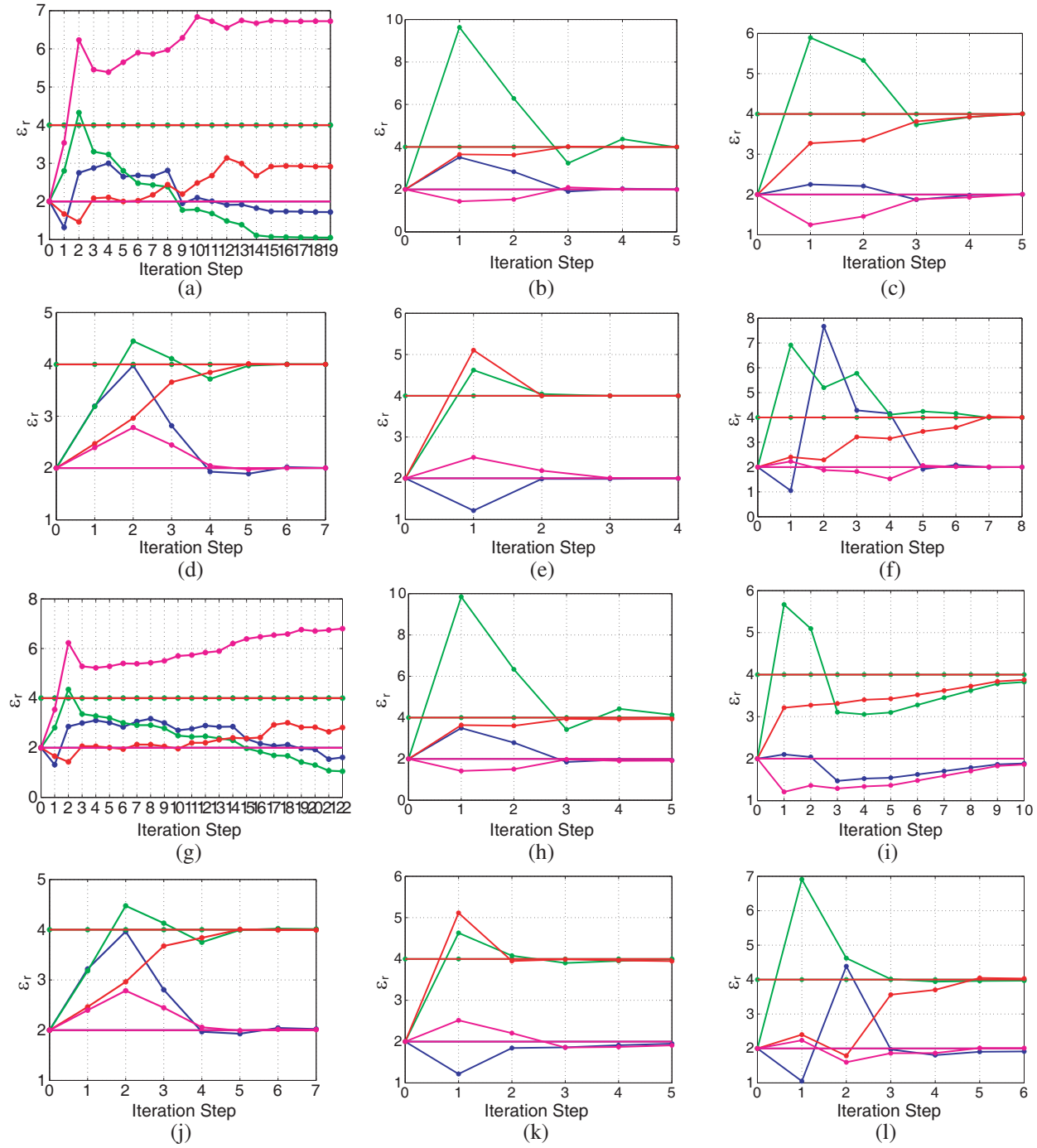

Figure 8. Inverted relative permittivities for anisotropic cubes from different transmitter-receiver polarizations when the receivers are at $y = 3.0\,\mathrm{m}$ and the transmitter is at $(0.5, 1.5, 0.5)\,\mathrm{m}$: solid line actual values, dotted line inverted values, blue line ϵ_{r1}, green line ϵ_{r1z}, red line ϵ_{r2}, purple line ϵ_{r2z}. First two rows: noiseless data; last two rows: noisy data. (a) y-x, (b) y-y, (c) y-z, (d) z-x, (e) z-y, (f) z-z, (g) y-x, (h) y-y, (i) y-z, (j) z-x, (k) z-y, (l) z-z.

4.3. Example 3: Reconstruction of Anisotropic Permittivities

In this example, the relative permittivities of the two cubes are chosen to be anisotropic. The permittivity tensors are $\epsilon_{r1} = 2.0, \epsilon_{r1z} = 4.0$ and $\epsilon_{r2} = 4.0, \epsilon_{r2z} = 2.0$ for the left and right cubes, respectively. We still consider two cases, which are when receivers are on the same side and different

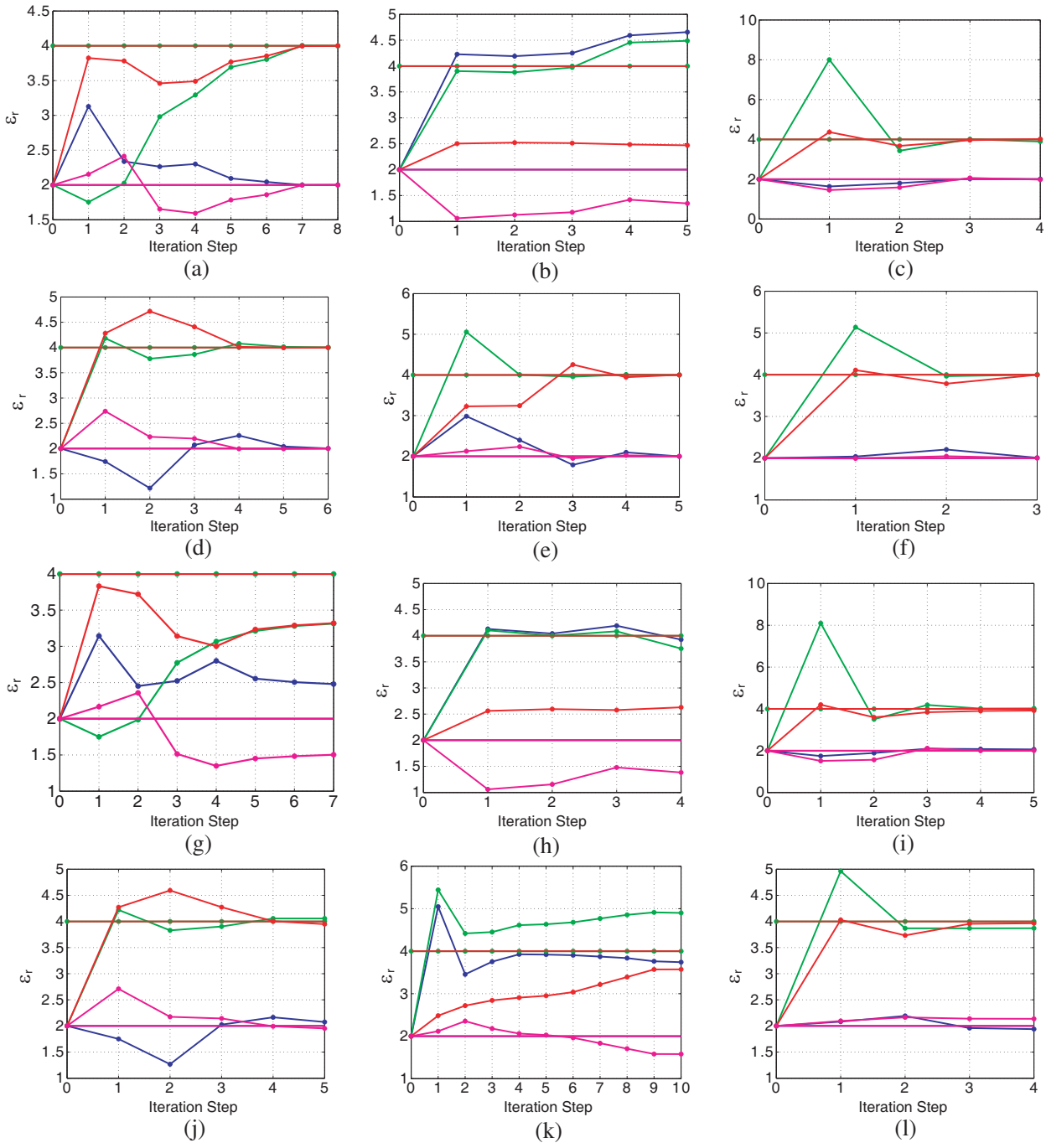

Figure 9. Inverted relative permittivities for anisotropic cubes from different transmitter-receiver polarizations when the receivers are at $y = -3.0\,\text{m}$ and the transmitter is at $(0.5, 1.5, 0.5)\,\text{m}$: solid line actual values, dotted line inverted values, blue line ϵ_{r1}, green line ϵ_{r1z}, red line ϵ_{r2}, purple line ϵ_{r2z}. First two rows: noiseless data; last two rows: noisy data. (a) y-x, (b) y-y, (c) y-z, (d) z-x, (e) z-y, (f) z-z, (g) y-x, (h) y-y, (i) y-z, (j) z-x, (k) z-y, (l) z-z.

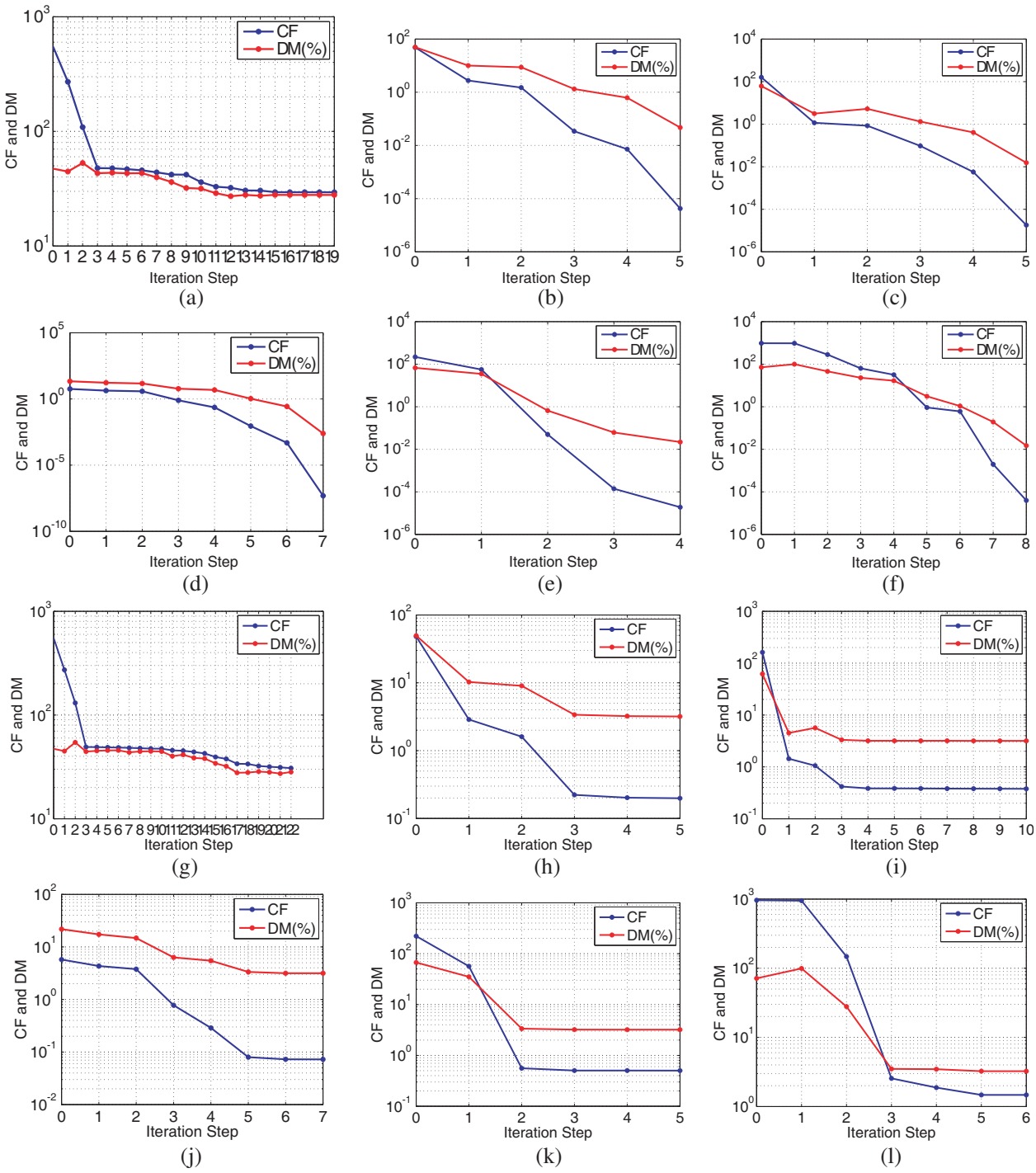

Figure 10. Cost function and data mismatch using data from different transmitter-receiver polarizations when the receivers are at $y = 3.0$ m and the transmitter is at $(0.5, 1.5, 0.5)$ m for anisotropic cubes: blue line CF, red line DM (%). First two rows: noiseless data; last two rows: noisy data. (a) y-x, (b) y-y, (c) y-z, (d) z-x, (e) z-y, (f) z-z, (g) y-x, (h) y-y, (i) y-z, (j) z-x, (k) z-y, (l) z-z.

sides of the transmitter. And we will still show the numerical results for both the noiseless and noisy data. For the noisy data, 25 dB SNR is applied again. The initial guess for the contrast permittivity tensor of each cube is chosen as the unit dyad $\overline{\mathbf{I}}$.

Figure 8 are the results when the transmitter and receivers on the same side. Fig. 9 shows the

inverted results when the transmitter and receivers on different sides. We can see that when the transmitter and receivers are on the same side, the inversion using the y-x polarized data stops in 19 steps for noiseless data and in 22 steps for noisy data, and the inversion does not converge. The reason

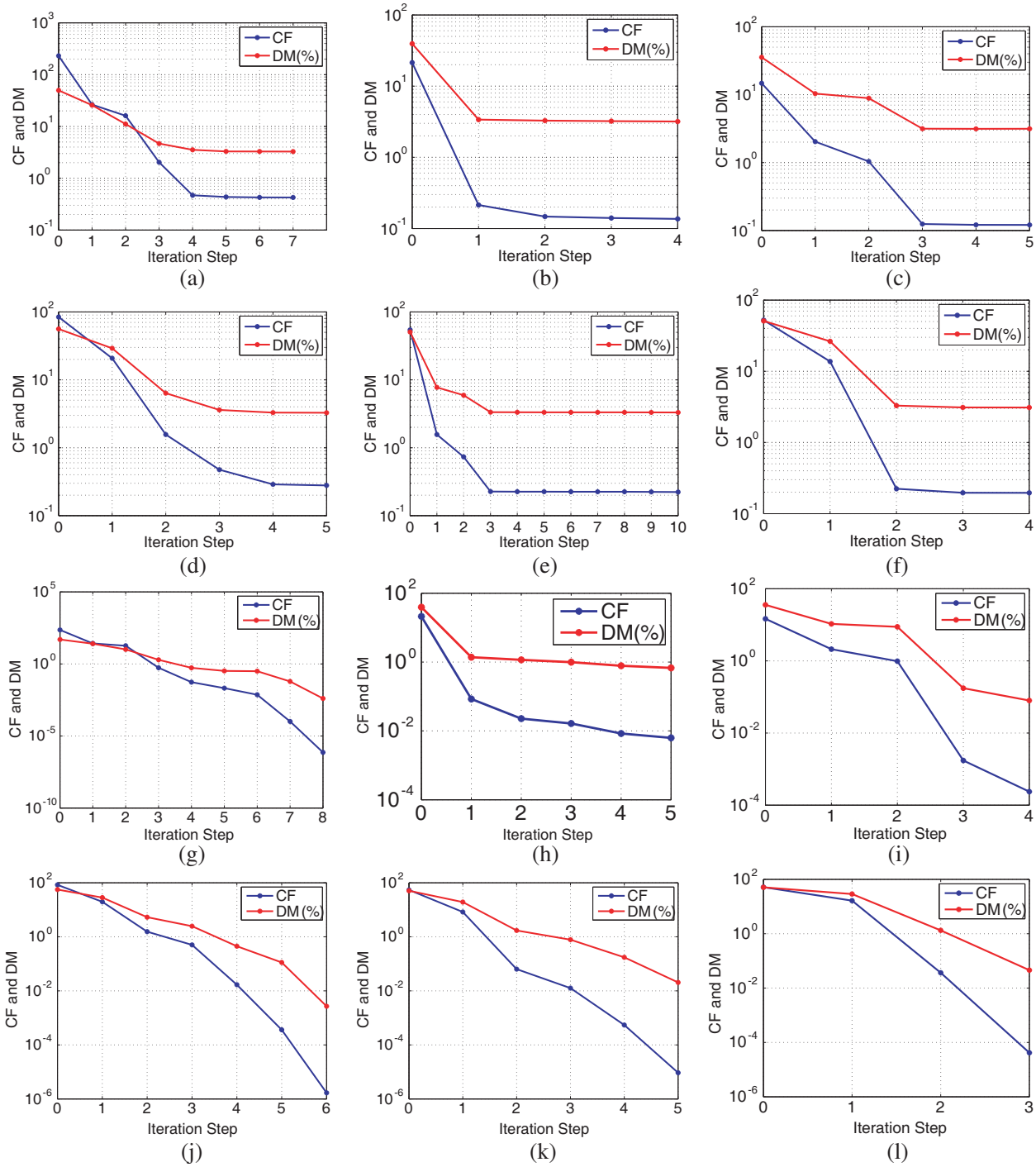

Figure 11. Cost function and data mismatch using data from different transmitter-receiver polarizations when the receivers are at $y = -3.0\,\mathrm{m}$ and the transmitter is at $(0.5, 1.5, 0.5)\,\mathrm{m}$ for anisotropic cubes: blue line CF, red line DM (%). First two rows: noiseless data; last two rows: noisy data. (a) y-x, (b) y-y, (c) y-z, (d) z-x, (e) z-y, (f) z-z, (g) y-x, (h) y-y, (i) y-z, (j) z-x, (k) z-y, (l) z-z.

for the stop of the iteration is that the difference of data mismatches in the two successive steps is within the defined tolerance. Similarly for the results when the transmitter and receivers are on different sides, the y-y polarized inversion for both the noiseless and noisy cases stops in about 5 steps due to the small change of the data mismatch in two successive steps. From these observations, we can conclude that the y-x and y-y polarized measurements lack the sensitivity to the anisotropic permittivities.

We also find that when the transmitter is z-polarized, the inversion results converge in 10 steps no matter the receivers are on the same side or different sides of the transmitter (Except that in Fig. 9, the inversion from the z-y polarization does not converge for the noisy case). Hence, it can be summarized that y-x and y-y measurements have weak sensitivity to the anisotropy when the anisotropic permittivity is isotropic in the x-y plane while changes in the z direction. In this case, z-polarized measurements such as y-z, z-x, z-y, z-z are more sensitive to anisotropy.

Next, we plot CF and DM for different cases. Fig. 10 shows the CF and DM as a function of iteration step when transmitter and receivers are on the same side. Fig. 11 show the results when transmitter and receivers are on different sides. As shown, some of the transmitter-receiver pairs lack sensitivity to the anisotropy, and cost function does not change as iteration proceeds for these cases. Also similar to the isotropic case, the DM converges to very small values for the noiseless data. While for the noisy data, the values cannot converge to the ones below the noise level.

4.4. Example 4: Reconstruction of Anisotropic Objects

In the this example, we consider two cubes with centers at $(0, -0.5, 0)$ and $(0, 0.5, 0)$ and side lengths of 1 m. The measurement data are generated by one of the cubes centered at $(0, 0.5, 0)$ only with relative permittivity of $\epsilon_r = 3$ and $\epsilon_{rz} = 6$. The frequency is 0.1 GHz. We then assume two cubes in the original model and invert their relative permittivities. The transmitters are electric dipoles located at 6 points at $(\pm 5.0, 0, 0)$, $(0, \pm 5.0, 0)$, $(0, 0, \pm 5.0)$ and polarized in the x, y, z directions at each point. The receivers are polarized in the z direction only and placed around the objects with a distance of 6 m from the origin. The azimuthal angle (ϕ) varies from 0 to 360° with step of 90°, and the polar angle (θ) varies from 0 to 180° with step of 10°. Fig. 12 shows the inversion results. We see that the relative permittivity of the first cube converges to an identity since the first cube does not exist in the synthetic model. The permittivity of the second cube is well reconstructed.

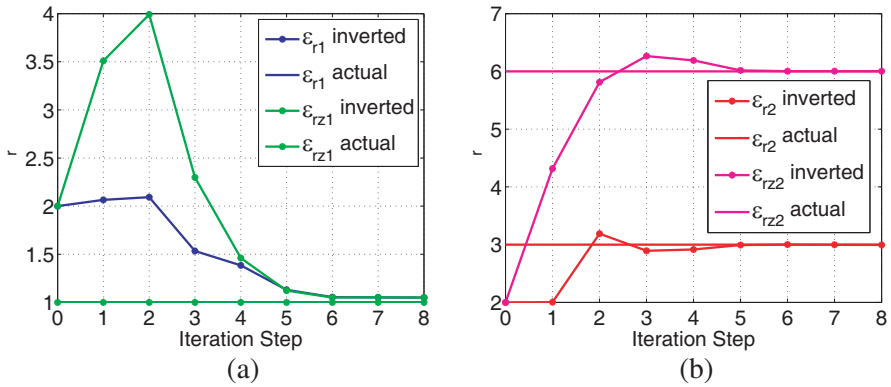

Figure 12. Inverted results of relative permittivities. (a) Cube1, (b) cube2.

5. CONCLUSION

The model-based inversion algorithm is applied to the reconstruction of anisotropic permittivities in free space. The inversion results are compared with isotropic permittivities. The results show that the inversion converges well for isotropic permittivities using the transmitter-receiver pairs with different polarizations. While for anisotropic permittivities, different polarized transmitter-receiver pairs have different sensitivities to the anisotropy. Some transmitter-receiver pairs are more sensitive to the

anisotropy than the others. Sensitivity analysis for different transmitter-receiver pairs are performed. The inversion results show that when there is enough sensitivity in the measurements, the anisotropic permittivities are reconstructed well. On the other hand, for less sensitive measurements, the inversion does not converge. Results from both the noiseless and noisy data are presented. The numerical results show good potential for the inversion of the geometry for the anisotropic objects using the model-based inversion method, which will be further investigated in the future.

ACKNOWLEDGMENT

The authors would like to thank Prof. W. C. Chew of Purdue University for his valuable instruction to the work.

REFERENCES

1. Chew, W. C. and Y. M. Wang, "Reconstruction of two-dimensional permittivity distribution using the distorted born iterative method," *IEEE Trans. on Medical Imaging*, Vol. 9, No. 2, 218–225, Jun. 1990.
2. Chew, W. C., *Waves and Fields in Inhomogeneous Media*, IEEE Press, 1995.
3. Li, F., Q. H. Liu, and L.-P. Song, "Three-dimensional reconstruction of objects buried in layered media using born and distorted born iterative methods," *IEEE Geoscience and Remote Sensing Letters*, Vol. 1, No. 2, 107–111, Apr. 2004.
4. Habashy, T. M. and A. Abubakar, "A general framework for constraint minimization for the inversion of electromagnetic measurements," *Progress In Electromagnetics Research*, Vol. 46, 265–312, Sep. 2004.
5. Abubakar, A. and P. M. van den Berg, "Three-dimensional nonlinear inversion in cross-well electrode logging," *Radio Sci.*, Vol. 33, 989–1004, Jul.–Aug. 1998.
6. Omeragic, D., L. E. Sun, V. Polyakov, Y.-H. Chen, X. Cao, T. Habashy, T. Vik, J. Rasmus and J.-M. Denichou, "Characterizing teardrop invasion in horizontal wells in the presence of boundaries using LWD directional resistivity measurements," *54th Annual Society of Petrophysicists and Well Log Analysts (SPWLA) Symposium*, Jun. 22–26, 2013.
7. Hu, Y., G. L. Wang, L. Liang, and A. Abubakar, "Estimation of reservoir parameters from inversion of triaxial induction data constrained by mud-filtrate invasion modeling," *IEEE Journal on Multiscale and Multiphysics Computational Techniques*, Vol. 2, 228–236, 2017.
8. Firoozabadi, R. and E. L. Miller, "A shape-based inversion algorithm applied to microwave imaging of breast tumors," *IEEE Trans. Antennas Propagat.*, Vol. 59, No. 10, 3719–3729, Oct. 2011.
9. Li, M., A. Abubakar, and T. M. Habashy, "A three-dimensional model-based inversion algorithm using radial basis functions for microwave data," *IEEE Trans. Antennas Propagat.*, Vol. 60, No. 7, 3361–3372, Jul. 2012.
10. Sun, L. E. and W. C. Chew, "A novel formulation of the volume integral equation for electromagnetic scattering," *Waves in Random and Complex Media*, Vol. 19, No. 1, 162–180, Feb. 2009.
11. Jin, J. M., *The Finite Element Method in Electromagnetics*, John Wiley & Sons. Inc., New York, 2002.